Bulletin of the Seismological Society of America, Vol. 99, No. 3, pp. 1906–1920, June 2009, doi: 10.1785/0120080019

Ⓔ

Automatic *S*-Wave Picker for Local Earthquake Tomography

by T. Diehl,* N. Deichmann, E. Kissling, and S. Husen

Abstract High-resolution seismic tomography at local and regional scales requires large and consistent sets of arrival-time data. Algorithms combining accurate picking with an automated quality classification can be used for repicking waveforms and compiling large arrival-time data sets suitable for tomographic inversion. *S*-wave velocities represent a key parameter for petrological interpretation, improved hypocenter determination, as well as for seismic hazard models. In our approach, we combine three commonly used phase detection and picking methods in a robust *S*-wave picking procedure. Information from the different techniques provides an *in situ* estimate of timing uncertainty and of the reliability of the automatic phase identification. Automatic picks are compared against manually picked reference picks of selected earthquakes in the Alpine region. The average accuracy of automatic picks and their classification is comparable with the reference picks, although a higher number of picks is downgraded to lower quality classes by the automatic picker. In the production-mode, we apply the picker to a data set of 552 earthquakes in the Alps recorded at epicentral distances $\leq$150 km. The resulting data set includes about 2500 *S* phases with an upper error bound of 0.27 sec.

Online Material: Details on the proposed automatic *S*-wave picking algorithm.

Introduction

Resolution and reliability of travel-time-based inversion techniques, like tomography and hypocenter determination, depend strongly on the consistency of the available arrival times. Because of an increasing number of available digital waveform data, modern repicking algorithms represent a possibility to derive consistent and large sets of arrival-time data. Because quality assessment is crucial for tomography applications, it represents an essential component of any automatic algorithm. Recent studies with repicked and automatically weighted *P*-phase data in Italy (Di Stefano *et al.*, 2006) and within the Alpine orogen (Diehl *et al.*, 2009) demonstrated the significant gain of resolution and reliability for tomographic velocity models at local to regional scales.

In terms of composition and physical state of the lithosphere, additional *S*-wave velocity models represent one of the key parameters. Independent measures of *P*- and *S*-wave velocities allow, for instance, the computation of the V_P/V_S ratio, which is proportional to the Poisson's ratio (Holbrook *et al.*, 1992; Christensen, 1996), and allow also better estimates on subsurface temperature (Goes *et al.*, 2000). Therefore, the quality weighted automated repicking of *S* waves represents the next step towards three-dimensional petrological models derived from seismic tomography. In addition, appropriate *S*-wave models and reliable *S* arrivals add important constraints to the earthquake location problem; in particular, focal depth depends critically on the use of *S* arrivals as demonstrated, for example, by Gomberg *et al.* (1990).

Onset determination of *S* waves, however, is difficult due to the character of the later arriving shear wave as described in the Ⓔ supplement that is available in the electronic edition of *BSSA*. Even manual picking and phase identification is often uncertain, especially at larger epicentral distances. On the other hand, we can make use of the characteristics of an *S* wave by exploiting the information of three-component (3C) recordings. The product of different polarization filters applied to a 3C recording, as presented by Cichowicz (1993), combines the major characteristics of an *S*-wave arrival into one single characteristic function (CF). Such a CF can be used for detection and picking of *S* phases because it is not sensitive to *P* phases. However, the method described by Cichowicz strongly depends on the assumption that incidence angle φ and back azimuth β can be derived from polarization analysis of the incoming *P* wave and that the *S* wave is linearly polarized.

Wang and Teng (1997) combined the approach of Cichowicz (1993) with additional *S*-wave attributes, like a change of autoregressive (AR) coefficients and the comparison of a short-term average (STA) against a long-term

*Present address: Lamont-Doherty Earth Observatory, Columbia University, Palisades, New York 10964

average (LTA). They use a pattern recognition technique to identify and pick *S* waves. A similar combined approach is used by Bai and Kennett (2000) to detect and identify regional *P* and *S* phases in 3C seismograms. They implement a polarization analysis based on complex traces derived from the Hilbert transform of the real part of the signal. The method proposed by Akazawa (2004) includes an iterative application of envelope functions, STA/LTA detectors, and AR picking algorithms based on the Akaike information criterion (AIC) (Akaike, 1973). Although these combined approaches result in high-detection rates and acceptable accuracy, they do not provide any uncertainty estimate of identification and timing, which is required for travel-time inversions.

In our approach we combine an *S*-wave detector similar to Cichowicz (1993) with an STA/LTA detector, which is applied to the original horizontal components and which, therefore, does not require a correct rotation of components. In addition, a predictive AR-AIC picking algorithm is used on single (original and rotated) components and on a combination of both horizontal components as described, for example, in Takanami and Kitagawa (1991) or Leonard and Kennett (1999). The information provided by the different picking techniques are combined to yield robust *S*-wave arrival times and are used to derive *in situ* estimates of the uncertainty and quality of the corresponding phase pick. We apply our *S*-wave picking approach to a data set of 3C recordings of local earthquakes in the Alpine region. Because our approach should mimic the manual picks of an analyst, a consistently hand picked reference data set is used to calibrate the parameters and to check the performance of the automatic picker in terms of accuracy and quality assessment. Subsequently, the calibrated picker is applied in the production mode to a data set of 552 events.

Combined Picking Approach

For stable and reliable *S*-wave picking, different *S*-wave attributes have to be combined. Our approach to an automatic *S* picker is based on three different detection and picking methods as summarized in the flow chart of Figure 1. An STA/LTA energy detector and a polarization detector are used to identify the first arriving *S* phase. The information provided by the detectors is used to setup the search windows of the AR-AIC picker. Finally, information from the detectors and AR-AIC picker is combined to yield the arrival-time tS_{me} of the first arriving *S* phase and its corresponding uncertainty interval defined by tS_{lo} and tS_{up}.

As minimum *a priori* information, the presented picking procedure requires an existing *P*-phase pick tP_{obs} (hand picked or high-quality automatic pick) and a predicted *S*-arrival time tS_{pre} (theoretical arrival time in an appropriate regional velocity model, usually one-dimensional *P*-wave velocities divided by a constant V_P/V_S ratio). Prior to any application, each component of the combined picking approach has to be calibrated with a set of reference *S* picks by a trial-and-error procedure as demonstrated in the Calibration and Test-Mode section.

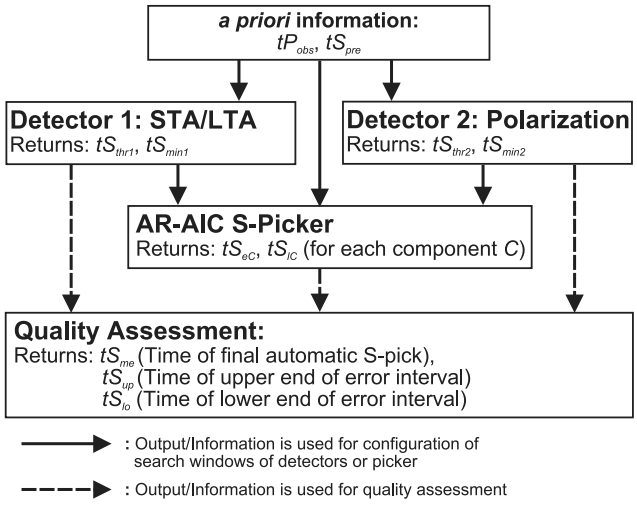

Figure 1. Flow chart of proposed automatic *S*-wave picking approach. The procedure requires *a priori* information on the *P*-wave arrival time tP_{obs} and on the predicted *S*-arrival time tS_{pre}. Information provided by detectors are used to setup the search windows of the AR-AIC picker and for automatic quality assessment. See Table 1 for further description of variables.

In the following paragraphs we describe the basic principles of the detectors, the AR-AIC picker, and the quality assessment. Ⓔ More detailed documentation on the methodology is presented in a supplement in the electronic edition of *BSSA*. Figures, tables, and equations provided in the supplement are indicated by the prefix "S." To facilitate the reader's orientation, the most important variables used in the following description are summarized in the glossary of Table 1.

STA/LTA Detector

The STA/LTA picker represents a very common and simple technique for phase detection. It is implemented in many online-detection algorithms, and its principles are described, for example, by Allen (1978, 1982), Berger and Sax (1980), or Ruud and Husebye (1992). Detectors based on STA/LTA are mainly sensitive to a change in amplitude (energy); and therefore discrimination between *P* and *S* phases is critical, even if applied only to horizontal components. In our implementation, we calculate running STAs and LTAs from the originally horizontal components (*E* and *N*), as described in the Ⓔ supplement that is available in the electronic edition of *BSSA*. The lengths of short-term (Δst) and long-term (Δlt) average windows basically control the resolution of the CF of the STA/LTA detector and have to be determined in the calibration procedure. To restrict the detection to possible *S* phases, we have to ensure that no *P* wave is present in the *S*-detection window. The proposed setup of the *S*-phase search windows uses tP_{obs} and tS_{pre} to determine a first coarse *S*-picking window. The coarse *S* window is used to

Table 1

Glossary of the Most Important Variables Used and Returned by the Different Detectors and Pickers

Variable	Description
General Variables	
tP_{obs}	Time of *a priori* (known) *P* arrival (e.g., from high-quality autopick)
tS_{pre}	Time of predicted *S* arrival (e.g., from velocity model)
t_{MHA}	Time of maximum horizontal amplitude y_{MHA}
tS_{me}	Time of final automatic *S* pick (from quality assessment)
tS_{up}	Time of upper bound of error interval (from quality assessment)
tS_{lo}	Time of lower bound of error interval (from quality assessment)
Variables Used/Returned by STA/LTA Detector	
tS_{thr1}	Time of threshold-based STA/LTA *S* pick (latest possible)
$tS_{min\,1}$	Time of minimum-based STA/LTA *S* pick (earliest possible)
Variables Used/Returned by Polarization Detector	
tS_{thr2}	Time of threshold-based polarization *S* pick (latest possible)
$tS_{min\,2}$	Time of minimum-based polarization *S* pick (earliest possible)
Variables Used/Returned for AR-AIC Picker	
t_{AC}	Time of initial pick for AIC configuration (from detectors or tS_{pre})
AIC^C	AIC function for component *C* ($C = N$, E, T, Q, or H); $H = E + N$
tS_{AC}	Time of AIC minimum for component *C* ($C = N$, E, T, Q, or H)
tS_{eC}	Time of earliest possible AIC pick for component *C*
tS_{lC}	Time of latest possible AIC pick for component *C*

determine the position of the maximum horizontal amplitude y_{MHA} at time t_{MHA} as illustrated in Figure 2. We expect the actual *S*-phase onset to occur certainly prior to t_{MHA}; and therefore the lower and upper end of the search window (*SW*1 and *SW*2, respectively) can be determined from the position of tP_{obs} and t_{MHA} as described in the Ⓔ supplement that is available in the electronic edition of *BSSA*. The picking algorithm applied to the characteristic STA/LTA function within the search window is similar to the method proposed by Baer and Kradolfer (1987). We extended their threshold-based method by a minimum-picking approach also suggested by Cichowicz (1993), where a (global) minimum of the CF prior to the threshold-based pick is determined. The threshold thr_1 is determined from the standard deviation σ_1 of the STA/LTA function within the search window as described in the Ⓔ supplement available in the electronic edition of *BSSA*. A pick is declared if the actual STA/LTA exceeds the threshold thr_1 and remains above the threshold for a minimum time *tup*. To account for roughness and singularities present in CFs derived from complex seismic

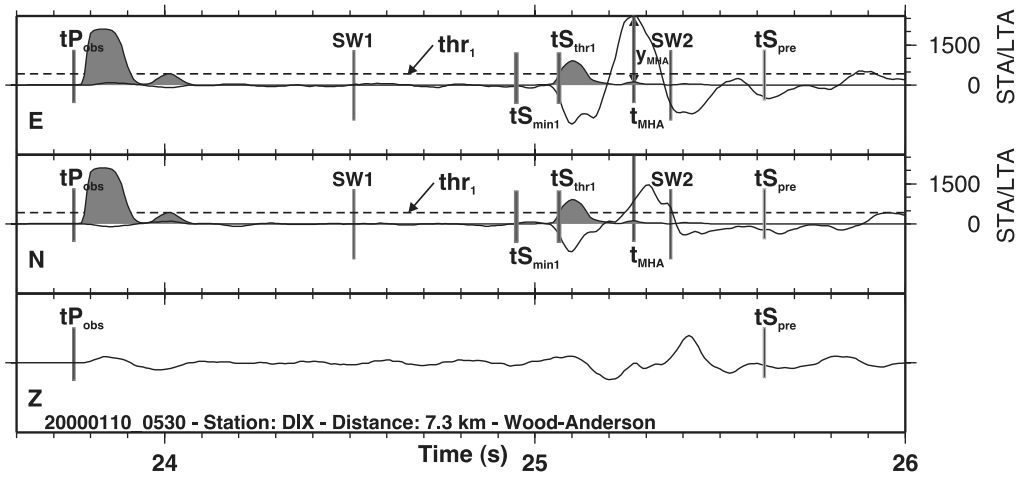

Figure 2. Combined STA/LTA approach used for *S*-wave detection on horizontal components. Black solid curves represent the Wood–Anderson filtered 3C seismograms (amplitudes normalized by station maximum) of a local earthquake in Switzerland (M_L 3.1, focal depth of 9 km). The gray shaded trace denotes the combined STA/LTA ratio derived from *N* and *E* components. tP_{obs} represents the known *P*-arrival time, and tS_{pre} indicates the position of theoretical *S* arrival predicted from a regional one-dimensional model. The dashed horizontal line denotes the dynamic threshold thr_1 for the picking algorithm. The *S*-wave arrival time based on the STA/LTA detector in the potential *S* window (*SW*1 to *SW*2) is most likely located in the interval between $tS_{min\,1}$ (minimum pick) and tS_{thr1} (threshold pick). See the text and Table 1 for further description.

signals, Baer and Kradolfer (1987) introduced the additional parameter *tdw*. The pick flag is not cleared if the CF drops below the threshold for a time interval less than *tdw*. Values for *tup* and *tdw* are determined in the calibration procedure. The corresponding threshold-based pick in Figure 2 is represented by tS_{thr1}.

Our minimum-picking approach determines the minimum value of the CF prior to tS_{thr1} and is equivalent to a delay correction usually necessary for threshold-based picks. The corresponding minimum pick is represented by $tS_{\mathrm{min\,1}}$ in Figure 2. Ⓔ Further details on the minimum-picking are provided in the supplement that is available in the electronic edition of *BSSA*.

Polarization Detector

Polarization filters as described, for example, by Flinn (1965) and Montalbetti and Kanasewich (1970) are commonly used to enhance the signal-to-noise ratio of seismic body waves. Rectilinearity (degree of linear polarization) and directivity of the particle motion are derived from eigenvalue analysis of the covariance matrix over small time intervals. Moreover, these time-domain filter operators can also be applied for identification of body phases because compressional and shear waves exhibit a high degree of linear polarization in contrast to any Rayleigh-type wave. For known azimuth and incidence of the incoming wave field, directivity of particle motion can be used to distinguish between compressional and shear waves. Cichowicz (1993) combined rectilinearity, directivity, and the ratio between transverse and total energy into one characteristic function CF_S, which is merely sensitive to *S*-wave energy and omits all *P* phases (*Pg*, *PmP*, *Sp*, etc.). The implementation of our polarization detector is mainly based on the approach of Cichowicz (1993), and its principles are briefly summarized in the following paragraphs.

As a first step, we determine the direction $\vec{L}$ of the incoming *P* wave. We compute the 3C covariance matrix within a narrow window around the known first arriving *P* phase tP_{obs}. The back azimuth β and the angle of incidence φ are derived from the eigenvector corresponding to the maximum eigenvalue of the covariance matrix. To separate *P* from *SV* and *SH* energy, we rotate the observation system defined by vertical (Z), north–south (N), and east–west (E) component of the seismometer into a ray-coordinate system defined by L-, Q-, and T-components (LQT) using rotation angles β and φ (Plešinger *et al.*, 1986). The L-component coincides with the principle direction of the *P*-wave particle motion, the T-component coincides with the transverse particle motion (*SH* energy), and the Q-component corresponds to a vector normal to L and T (*SV* energy).

Finally, we calculate the directivity $D(t)$, the rectilinearity $P(t)$, the ratio between transverse and total energy $H(t)$, and a weighting factor $W(t)$ within a centered window for each sample of the rotated time series. The length of the polarization filter used to analyze a seismogram is derived empirically from the observation-quality *qP* of the *P* phase (Ⓔ for further details on window lengths see the supplement that is available in the electronic edition of *BSSA*). The covariance matrix is determined from the centered window for each sample.

Directivity $D(t)$ is defined as the normalized angle between $\vec{L}$ and eigenvector $\vec{\epsilon}_{\mathrm{max}}$ corresponding to the maximum eigenvalue of the covariance matrix. The directivity operator is expected to be close to zero for the first arriving *P* wave ($\vec{\epsilon}_{\mathrm{max}}$ parallel to $\vec{L}$) and close to one for the first arriving *S* wave ($\vec{\epsilon}_{\mathrm{max}}$ perpendicular to $\vec{L}$). Rectilinearity $P(t)$ is calculated using the formulation of Samson (1977), and it is expected to be close to one for both first arriving *P* and *S* waves. The ratio between transverse and total energy $H(t)$ within the centered window is expected to be close to one for the first arriving *S* wave and zero for the first arriving *P* wave. As an addition to the original method of Cichowicz (1993), we calculate a weighting factor $W(t)$ for each window, which accounts for the absolute amplitude within the centered window with respect to the maximum amplitude derived from the coarse *S* window.

The product of the three squared filter operators with the weighting factor $W(t)$ yields the modified CF for *S*-wave detection CF_S:

$$\mathrm{CF}_S(t) = D^2(t)P^2(t)H^2(t)W(t). \tag{1}$$

Figure 3 shows the LQT components of the same local earthquake from Figure 2 and the corresponding *S*-wave operators $D(t)$, $P(t)$, and $H(t)$. The arrival of the *S* wave (gray band) goes along with the simultaneous increase of $D(t)$, $P(t)$, and $H(t)$ and leads to a well-defined signature on CF_S.

The picking algorithm applied to CF_S is almost identical to the one used for the STA/LTA detector described previously. Ⓔ A detailed description of the picking algorithm can be found in the supplement that is available in the electronic edition of *BSSA*. The threshold thr_2 for the picker is derived from the standard deviation and the mean of CF_S within a defined window similar to the procedure proposed by Cichowicz (1993). An additional water level term *cw* was introduced, which stabilizes the picking in case of a large signal-to-noise ratio. Values for *cw*, *tup*, and *tdw* are determined in the calibration procedure. The threshold-based pick on CF_S is represented by tS_{thr2} in Figure 3. In addition, we perform the minimum-picking prior to tS_{thr2} as described earlier to account for smaller precursory signals. The position of the minimum pick is marked as $tS_{\mathrm{min\,2}}$ in Figure 3. Compared to the actual arrival on the transverse component, tS_{thr2} and $tS_{\mathrm{min\,2}}$ are shifted by approximately 0.1 sec to earlier times (Fig. 3). This time shift is caused by the finite length of the polarization filter. For emergent arrivals the time shift is less significant.

Autoregressive Picker

AR models are very useful for the analysis of stationary time series. The nonstationary character of seismic signals

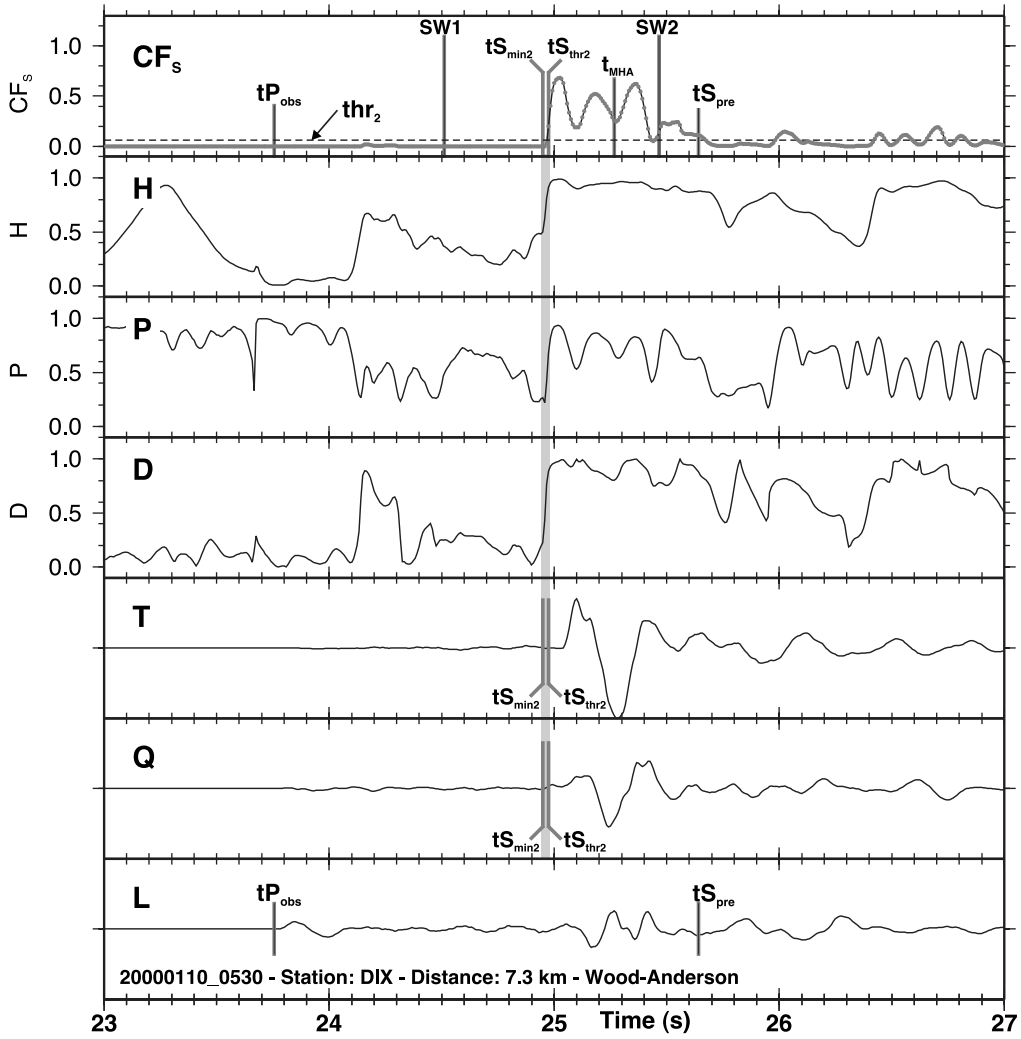

Figure 3. Example for the polarization detector applied to the same local earthquake as in Figure 2. L, Q, and T denote the rotated components. The corresponding S-wave operators are $D(t)$ (directivity), $P(t)$ (rectilinearity), and $H(t)$ (transverse to total energy ratio). The uppermost trace represents the amplitude weighted characteristic S-wave function CF_S. The arrival of the S wave (gray band) goes along with the simultaneous increase of $D(t)$, $P(t)$, $H(t)$, and CF_S. Compared to the actual arrival on T, the S-wave detection is shifted by approximately 0.1 sec to earlier times. This time shift is caused by the finite length of the polarization filter. CF_S is not affected by the P wave. See the text and Table 1 for further description.

can be approximated by dividing a time series into locally stationary segments each modeled as an AR process (Kitagawa and Akaike, 1978). Because the corresponding models are expected to be different before and after the arrival of a signal, such AR models can be used to automatically pick the arrival time of seismic phases by finding the time that attains the minimum AIC (Akaike, 1973) value of a locally stationary AR model.

Theory and implementation of different AR-AIC picking algorithms are described, for example, in Takanami and Kitagawa (1991), Leonard and Kennett (1999), or Sleeman and van Eck (1999). Although multivariate AR approaches appear to be slightly more appropriate for robust S-wave picking (e.g., Takanami and Kitagawa, 1993; Leonard and Kennett, 1999), the application of the univariate method to single components (N, E, Q, and T) and combined components ($E + N$) provides additional details about uncertainty of timing and phase identification. Our implementation is mainly based on the method of Takanami and Kitagawa (1988), which uses an univariate AR fitting approach to derive automatic arrival times. Ⓔ A detailed description of the AR modeling is provided in the supplement that is available in the electronic edition of *BSSA*.

In practice, the method of Takanami and Kitagawa (1988) requires a noise model $\mathrm{AIC}_i^{\mathrm{forw}}$ calculated forward in time starting at t_{NS} and ending at t_{SS}, assuming the noise part is included in the window from t_{NS} to t_{NE} as illustrated in the lower box of Figure 4. In addition, the signal model $\mathrm{AIC}_i^{\mathrm{back}}$ is calculated backward in time starting at t_{SE} and ending at t_{NE}, where parts of the signal are expected to

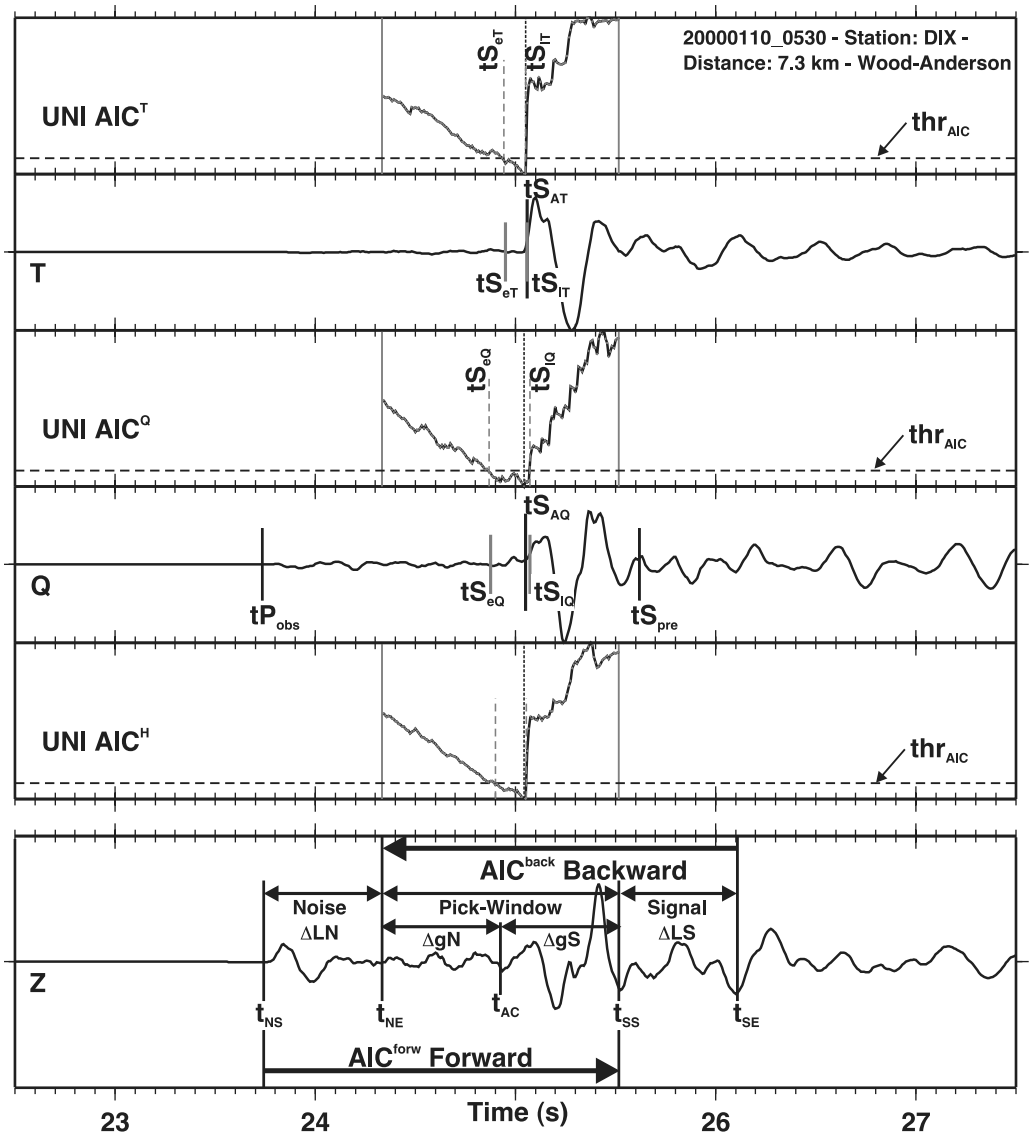

Figure 4. Example of the AR-AIC picker applied to the same local earthquake as in Figure 2. All amplitudes are trace normalized. The lower box illustrates the search window configuration centered around t_{AC}. The corresponding univariate AIC functions are shown for the combination of original $E + N$ components (AIC^H) and for the rotated components Q (AIC^Q) and T (AIC^T). AR-AIC picks tS_{AQ} and tS_{AT} derived from the minimum on the AIC functions agree very well with the actual arrival of the S wave visible on the seismograms. The uncertainty of the AR-AIC pick is expressed by the earliest and latest possible arrival times tS_{eQ}, tS_{eT}, tS_{lQ}, and tS_{lT} derived from intersection of threshold thr_{AIC} (dashed horizontal lines) with the corresponding AIC functions. See the text and Table 1 for further description.

be included in the window between t_{SS} and t_{SE}. By simply adding AIC_i^{forw} and AIC_i^{back} for common samples of the time series, we obtain the AIC_i of the locally stationary AR model. If i_{min} corresponds to the sample of the minimum AIC_i value, then $i_{min} + 1$ represents the best estimate of the arrival time. Moreover, AIC_i from different components can be added to give combined AIC functions; for example, AIC^H represents the sum of the horizontal components N and E. In Figure 4, the AIC functions have the typical shape with well-developed minima around the actual onset of the S wave. The AR-AIC estimated picks tS_{AQ} and tS_{AT} agree very well with the arrival observed on the different components. The onset appears more impulsive on the T component, which is also indicated by the sharper minimum on AIC^T compared to the one observed on AIC^Q.

Because of their fundamental concept, predictive AR-AIC pickers always require an initial pick t_{AC} to set up a noise model window ΔLN and signal model window ΔLS separated by the picking window $\Delta gN + \Delta gS$ (Fig. 4). Previous implementations of AR-AIC pickers, such as Sleeman and van Eck (1999) or Akazawa (2004), mainly use triggers from STA/LTA detectors and fixed window lengths for this purpose. The quality of AR-AIC pickers, however, depends strongly on the degree of separation

between noise and signal in the analysis window from t_{NS} to t_{SE} as discussed by Zhang *et al.* (2003). This can be critical if several phases are present within the window (e.g., *Pg* and *Sg* at very short epicentral distances or *Sn* and *Sg* at larger distances). Figures S4 and S5 (Ⓔ available in the supplement in the electronic edition of *BSSA*) present examples of such misconfigured AR-AIC search windows.

To avoid such misconfigured windows, minimum *a priori* information is required to guide the picker to the correct phase and to set up the AR-AIC search windows properly. Ⓔ We implemented a distance-dependent procedure for a dynamic configuration of AR-AIC search windows as described in the supplement that is available in the electronic edition of *BSSA*. Basically, tP_{obs} and information from both detectors are used for AR-AIC configuration at near-by epicentral distances. For distances $\geq \Delta_{\mathrm{AIC}_1}$ the AR-AIC configuration is mainly based on the predicted arrival time tS_{pre}. Above Δ_{AIC_3}, the usually weak *Sn* phase is expected to be the first arriving *S* wave. The correct identification requires a modified setup using information from detectors and tS_{pre}. Values for Δ_{AIC_1} and Δ_{AIC_3} have to be determined in the calibration procedure.

Quality Assessment in Combined Approach

Quality assessments implemented in the automatic picking procedures (Fig. 1) have to provide realistic estimates on the timing uncertainty of a pick, as well as minimum information on actual phase identification. Sophisticated pattern recognition methods used, for example, by Aldersons (2004) usually classify the quality of the onset based on wavelet characteristics in the close vicinity of the automatic pick. These methods, however, do not yet provide information on the phase type, in particular if it is a first or later arriving phase.

Robust uncertainty estimates for automatic *S* arrivals can be obtained by combining picking information from different techniques to define the lower tS_{lo} and upper tS_{up} limit of the error interval. The mean position of this interval $tS_{\mathrm{me}} = (tS_{\mathrm{up}} + tS_{\mathrm{lo}})/2$ is defined as the *S*-arrival time. In our approach, the earliest and latest possible pick from the STA/LTA detector ($tS_{\mathrm{min}\,1}$ and tS_{thr1}), polarization detector ($tS_{\mathrm{min}\,2}$ and tS_{thr2}), and the different AIC minima (tS_{AC}, with $C = N, E, Q, T$, and H) constitute the lower and upper limits of the corresponding error interval.

In addition, the width of the AIC minimum is usually related to the quality of the onset. Impulsive wavelets like the *S* arrival on the *T* component in Figure 4 lead to a distinct AIC minimum, whereas emergent wavelets produce broader minima (*Q* component in Fig. 4). The width of the AIC minimum can therefore be used as additional quality information about the arrival time and is also a good indicator for the presence of possible precursory phases. We define the earliest possible arrival derived from the AIC function as the first sample where AIC drops below the threshold $\mathrm{thr}_{\mathrm{AIC}}$ and the latest possible arrival as the last sample below $\mathrm{thr}_{\mathrm{AIC}}$ (see Fig. 4). Ⓔ The definition of threshold $\mathrm{thr}_{\mathrm{AIC}}$ is provided in the supplement that is available in the electronic edition of *BSSA*. The corresponding positions of earliest possible and latest possible arrivals are represented by tS_{eT}, tS_{eQ}, tS_{lT}, and tS_{lQ}. The usage of the AIC-quality assessment becomes especially important for appropriate uncertainty estimates at larger epicentral distances. In the following, we define the distance Δ_{AIC_2} above which the AIC quality assessment is considered for the overall quality assessment.

Because detectors and components are sensitive to different phase types in different distance ranges, we set up four different weighting scenarios based on tests with the reference data set. Ⓔ The weighting scenarios are described in further detail in the supplement that is available in the electronic edition of *BSSA*. The basic principles are summarized in Table 2. The error interval derived from the appropriate weighting scenario is used to calculate the mean position of the *S*-wave arrival and to assign a discrete quality class according to an *a priori* user-defined weighting scheme. Finally, a minimum amplitude signal-to-noise ratio $S2N_{\mathrm{min}}(m)$ is defined for each quality class m. If the signal-to-noise ratio of the current pick is less then $S2N_{\mathrm{min}}(m)$, the pick is downgraded to the next lower quality class, and its signal-to-noise ratio is checked again for the new class. Because we expect smaller signal-to-noise ratios for potential *Sn* phases, we define different sets of $S2N_{\mathrm{min}}(m)$ above and below Δ_{AIC_3}. Figure 5 shows examples for different automatic *S*-wave arrival picks and their corresponding error intervals at local to regional distances (Ⓔ further examples are provided in Figure S6 in the supplement that is available in the electronic edition to *BSSA*). The mean position and the error intervals of the automatic picks agree very well with the actual *S*-wave arrival observed on the seismograms.

Provided that a reliable origin time t_0 exists, we can define an expected *S* window from the arrival time of the *P* phase tP_{obs}, a minimum V_P/V_S ratio κ_{min}, and a maximum V_P/V_S ratio κ_{max}. Assuming a similar ray path for the *P* and *S* waves, the earliest possible *S* arrival is defined by $S_{\mathrm{lo}} = (tP_{\mathrm{obs}} - t_0)\kappa_{\mathrm{min}}$ and the latest possible *S* arrival is defined by $S_{\mathrm{up}} = (tP_{\mathrm{obs}} - t_0)\kappa_{\mathrm{max}}$. Automatic picks outside this expected *S* window will be rejected. Such a V_P/V_S filter reduces the number of mispicks due to phase misidentification. Because we expect larger variations in V_P/V_S for crustal phases at smaller epicentral distances (major part of the ray path within a heterogeneous upper crust), we define different V_P/V_S ranges above and below Δ_{AIC_3}.

Case Study: Application to the Alpine Region

Before an automatic picker can be applied to a large (unpicked) data set in a production mode, its performance has to be tested and compared with a smaller number of consistent reference hand picks in a test mode as described, for example, by Di Stefano *et al.* (2006) and Diehl *et al.*

Table 2
Summary of Quality Weighting Scenarios

		Scenario 1	Scenario 2	Scenario 3	Scenario 4
Epicentral distance Δ_{epi}		$< \Delta_{AIC_3}$	$< \Delta_{AIC_3}$	$\geq \Delta_{AIC_3}$	≥ 0 km
Expected first *S* phase		*Sg*	*Sg*	*Sn*	any
STA/LTA detection		?*	+†	?*	—‡
Polarization detection		+†	—‡	?*	—‡
STA/LTA	$tS_{min\,1}$		X§		Rejected
	tS_{thr1}		X§		
Polarization	$tS_{min\,2}$	X§			
	tS_{thr2}	X§			
AR-AIC	tS_{AH}	X§	X§	X§	
	tS_{eH}	O#	O#	X§	
	tS_{lH}			X§	
	tS_{AT}	x‖	X§	X§	
	tS_{eT}	o**	O#	X§	
	tS_{lT}			X§	
	tS_{AQ}	x‖	X§	X§	
	tS_{eQ}	o**	O#	X§	
	tS_{lQ}			X§	
	tS_{AN}		X§	X§	
	tS_{eN}		O#	X§	
	tS_{lN}			X§	
	tS_{AE}		X§	X§	
	tS_{eE}		O#	X§	
	tS_{lE}			X§	

See text and Ⓔ the supplement that is available in the electronic edition of *BSSA* for further details on how final *S* pick and associated quality class is computed. For further description of variables see Tables 1 and 4.

*? indicates that the detection of an *S* wave is possible.

†+ indicates the detection of an *S* wave.

‡— indicates no detection of an *S* wave.

§X indicates that the time was used for quality assessment.

‖x indicates that the time was used for quality assessment if the time is closest to $tS_{min\,2}$.

#O indicates that the time was used for quality assessment if $\Delta_{epi} \geq \Delta_{AIC_1}$.

**o indicates that the time was used for quality assessment if $\Delta_{epi} \geq \Delta_{AIC_1}$ and if the time is closest to $tS_{min\,2}$.

(2009). This procedure also involves the iterative calibration of the previously described picker components. The reference data set and the calibration procedure are summarized in the following sections. Subsequently, we present results of the production mode applied to 552 local earthquakes in the Alpine region. The waveform data set used for this case study is described in more detail in Diehl *et al.* (2009).

Reference Data Set

Our reference data set consists of 3C recordings of 49 local earthquakes in the greater Alpine region (white stars in Fig. 6). Because information on sensors and data loggers were not available for large parts of the data set, the instrument response could not be removed prior to the (reference as well as automatic) picking process. Sampling rates of the seismograms used in this study vary between 50 and 250 Hz. We considered epicentral distances $\Delta_{epi} \leq 150$ km for this test. Above the 150 km distance, visual identification and picking *S* waves becomes rather uncertain; and therefore it is difficult to compare manual picks with automatic picks.

For the reference *S* picking we considered the original Z-, N-, and E-components as well as rotated radial and transverse components. Each phase pick is associated with an uncertainty in timing and phase identification as described in Diehl *et al.* (2009). The reference data set features certainly a higher level of consistency than routinely determined *S*-wave picks provided in standard bulletin data. However, particular quality checks (e.g., Wadati diagrams) were not performed, and as a consequence the reference data may also contain some misidentified arrivals.

Table 3 shows the weighting scheme used for reference *S*-wave picking and the numbers of reference picks for each class. From 797 potential *S* waves to pick ($\Delta_{epi} \leq 150$ km, 3C recording, and existing *P* pick), 609 (76.4%) are classified as usable qualities (class 0–2). The rest are rejected (class 3). Ⓔ The estimated average picking uncertainty can be derived from the number of picks and the uncertainty interval of each class as described by equation (S17) in the supplement that is available in the electronic edition of *BSSA*. If we

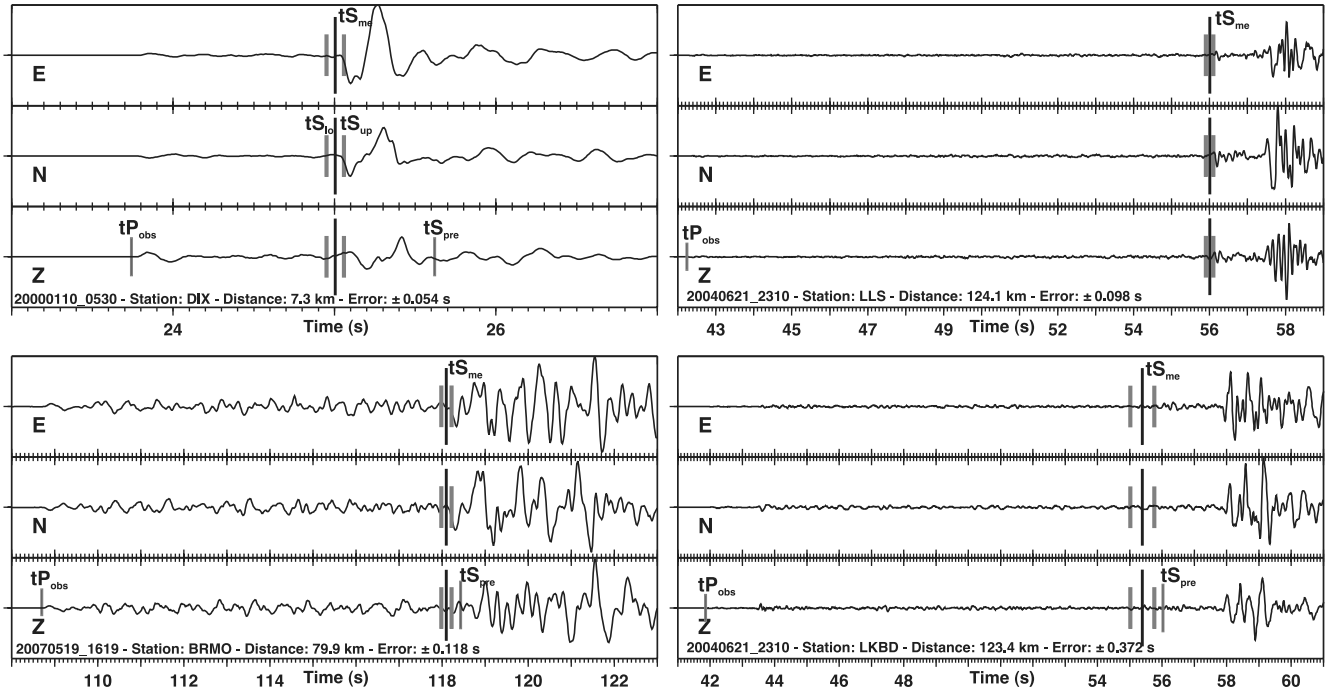

Figure 5. Examples of automatic *S*-wave picks at epicentral distances dominated by first arriving *Sg* phases (left-hand column) and first arriving *Sn* phases (right-hand column) for different error intervals. The error interval derived from the automatic quality assessment is represented by the vertical gray bars. The vertical long black bars denote the mean position of the *S*-wave onset. Error interval and mean position agree very well with the actual *S*-wave arrival observed on the seismograms.

consider only picks of usable quality classes, the average picking uncertainty of the reference data set is about 0.23 sec.

Calibration and Test Mode

The calibration of our picking approach basically consists of an iterative trial-and-error procedure. Parameters of the picking components have to be iteratively adjusted until the resulting performance fulfills the requirements for use in high-resolution tomography as described by Di Stefano *et al.* (2006) and Diehl *et al.* (2009). The assessment of the picker performance for a given set of (appropriate) parameters is described in the following section. Some guidelines on how a set of appropriate parameters is derived for a certain data set is provided at the end of the Calibration and Test Mode section.

Assessment of Picker Performance. We applied the automatic picking approach to the waveforms of the reference data set and compared timing and error assessment against reference picks. Predicted *S*-arrival times are calculated in the regional minimum one-dimensional *P*-wave model of Diehl *et al.* (2009) divided by a constant V_P/V_S ratio of 1.70. The corresponding hypocenters are relocated in the same minimum one-dimensional model as described by Kissling (1988) or Husen *et al.* (1999) using only *P* arrivals. The optimal performance was obtained with the picking parameters summarized in Table 4. The suggested values are derived from a parameter search, which is described subsequently.

The resulting performance of the automatic picker and the error assessment can be displayed in matrix form, as illustrated in Figure 7. A satisfactory automatic picking and quality assessment is achieved if the deviation between the automatic and reference picks is within the error interval of the corresponding automatic quality classification ($\sigma_{ij} \leq \varepsilon_j$ and $\sigma_j \leq \varepsilon_j$) and if only a few low-quality reference picks are upgraded to higher quality classes by the automatic picker (Fig. 7). Both requirements are satisfied with our automatic picker. All σ_j are less than or equal to ε_j (lowermost row of Fig. 7) and none of the reference class 3 picks (rejected class) is upgraded to the high-quality class 0 or 1 (dark shaded matrix-fields in Fig. 7). Only two reference picks that were rejected (not picked due to complicated waveforms) were upgraded to class 2 by the automatic picker. Furthermore, we observe no significant systematic bias between automatic picks and reference picks (lowermost row of Fig. 7). The mean value of ΔAR seems slightly negative (automatic earlier than reference pick) for highest quality class 0. For lower quality classes, automatic picks tend to be marginally delayed in comparison to reference picks. The upper limit of the average uncertainty for all usable automatic picks can be estimated as described earlier. We obtain an average uncertainty of 0.27 sec, which is only 40 msec larger than the average uncertainty derived from the reference picks.

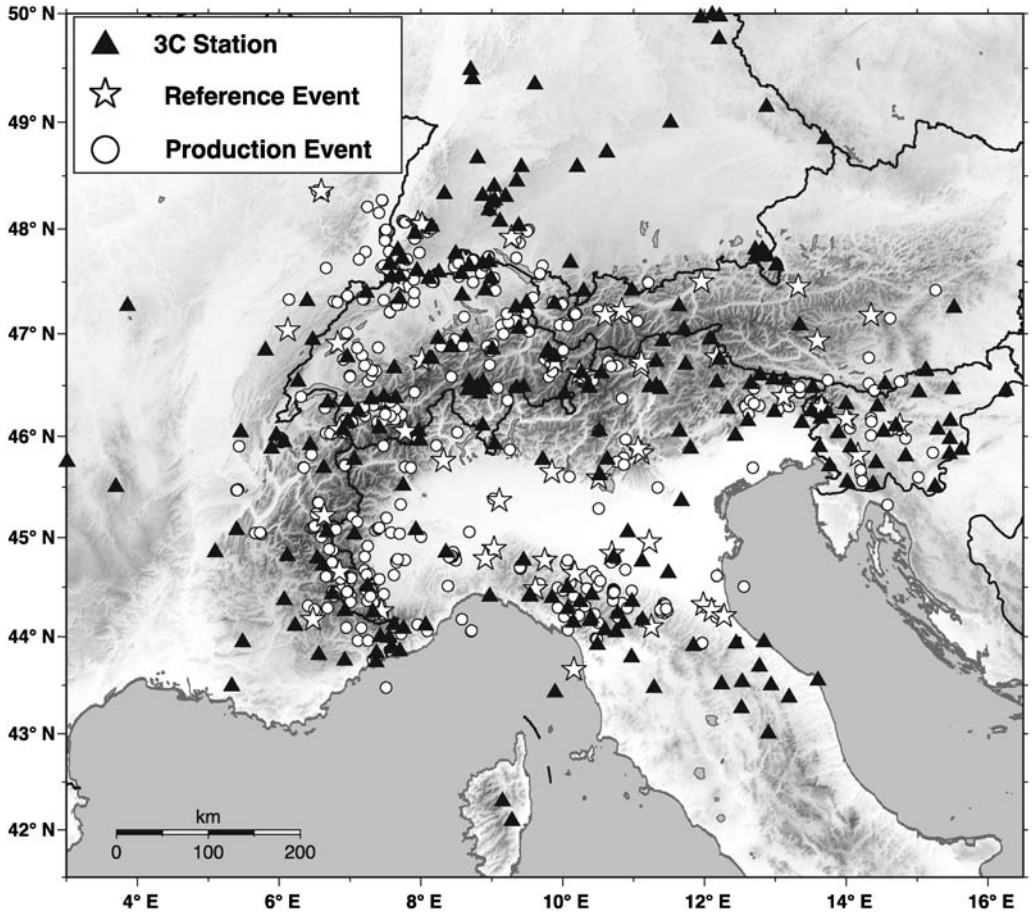

Figure 6. Map of 3C stations and earthquakes in the Alpine region used for the case study. Black triangles indicate stations, white stars denote locations of reference events used for the calibration of the picker, and white circles correspond to events used for the production mode.

Although the accuracy of the automatic picker is comparable to the reference picks, the automatic picker downgrades a large number of potential high-quality picks to lower classes (Fig. 7). Especially for class 1 and 2 more than half of the reference picks are rejected by the automatic picker. In addition, the recovery rate of 11% for class 1 is rather low compared to classes 0 (38%) and 2 (20%).

Ⓔ As discussed in the supplement that is available in the electronic edition of *BSSA*, an appropriate weighting scheme for seismic tomography can be achieved by merging classes 0 and 1. The simplified weighting scheme contains only two usable classes (0 and 1) and one reject class (2), as illustrated in Table S3. The highest quality represents the largest populated class, and the average picking uncertainty adds up to about 0.29 sec in this new weighting scheme (only slightly higher than the average uncertainty in the original weighting scheme). Such a well-balanced weighting scheme facilitates the model parametrization for tomography. On the other hand, the original weighting scheme of Figure 7 is more suitable for earthquake location problems because it

Table 3

Weight Assignments Based on Picking Errors for Reference *S* Waves from 49 Local and Regional Earthquakes in the Greater Alpine Region

S-Quality Class qS	Error ε_{qS} (sec)	Weight (%)	Number of Reference Picks
0	±0.10	100	153 (19.2%)
1	±0.20	50	280 (35.1%)
2	±0.40	25	176 (22.1%)
3	> 0.40	0 (rejected)	188 (23.6%)
Usable classes: 0–2 (76.4% of potential *S* phases)			
Average picking uncertainty of usable reference phases: 0.23 sec			

Number of reference picks refer to epicentral distances ≤ 150 km and potential *S* phases to pick (3C recording and existing *P* pick).

Table 4

Summary of Basic Parameters That Have to be Adjusted for the Described Picking Approach

Parameter	Description	Value
General Parameters		
$\Delta_{\text{epi}}^{\text{max}}$	Maximum epicentral distance	150 km
Δ_{AIC_3}	Distance above which *Sn* is expected as first arrival	100 km
Parameters for STA/LTA Detector		
Δst	Length of short-term window	0.2 sec
Δlt	Length of long-term window	2.0 sec
tup	Minimum time CF above threshold	0.05 sec
Parameters for Polarization Detector		
cw	Water level to stabilize the picking	0.06
tup	Minimum time CF_S above threshold	0.10 sec
tdw	Maximum time CF_S drops below threshold	0.05 sec
Parameters for AR-AIC Picker		
Δ_{AIC_1}	Distance above which predicted *S* is used for configuration	70 km
ΔgN, ΔgS	Initial length of picking window (before/after t_{AC})	1.0 sec
ΔLN, ΔLS	Initial length of noise/signal model window	1.0 sec
Parameters for Quality Assessment		
Δ_{AIC_2}	Distance above which AIC-quality is considered	50 km
$S2N_{\text{min}}^1$ (0)	Minimum signal-to-noise ratio for class 0 ($\Delta_{\text{epi}} < \Delta_{\text{AIC}_3}$)	3
$S2N_{\text{min}}^1$ (1)	Minimum signal-to-noise ratio for class 1 ($\Delta_{\text{epi}} < \Delta_{\text{AIC}_3}$)	3
$S2N_{\text{min}}^2$ (0)	Minimum signal-to-noise ratio for class 0 ($\Delta_{\text{epi}} \geq \Delta_{\text{AIC}_3}$)	3
$S2N_{\text{min}}^2$ (1)	Minimum signal-to-noise ratio for class 1 ($\Delta_{\text{epi}} \geq \Delta_{\text{AIC}_3}$)	2

The suggested values are derived from a parameter search that compares automatic picks with reference picks of local earthquakes within the greater Alpine region as described at the end of the Calibration and Test-Mode section.

contains *S* arrivals of high accuracy (class 0, ±0.1 sec), which are assigned with a higher uncertainty of ±0.2 sec in the merged weighting scheme. In the earthquake location problem, *S* arrivals of high accuracy significantly reduce the location uncertainty.

To assess the performance of the automatic picker especially regarding systematic mispicks and outliers present in the test-mode, we display the difference between automatic and reference *S* picks (ΔAR) for usable automatic picks against epicentral distance in Figure 8. In general, the number of outliers is low and the corresponding errors are large. The number of gross outliers increases in the distance range of the triplication zone (Fig. 8), due to misinterpretation of later arriving phases such as *Sg* or *SmS*.

An additional technique to identify mispicked *S* arrivals is the use of Wadati diagrams as described, for example, by Kisslinger and Engdahl (1973) or Maurer and Kradolfer (1996). Ⓔ Examples and results of such procedures are provided and discussed in the supplement that is available in the electronic edition of *BSSA*. The modified Wadati diagram of Figure S7b in the supplement suggests difficulties and ambiguity in manually picking and identifying *S* waves, especially beyond the crossover distance between *Sn* and *Sg*. On the other hand, the more conservative quality assessment of the automatic approach significantly reduces the scatter in *S*-phase arrivals (Fig. S7a in the supplement) at the cost of a lower number of usable picks. Finally, we point out that prior to any final velocity model estimation, the consistency of the automatic *S* picks have to be evaluated in an iterative inversion procedure as described, for example, by Kissling (1988) or

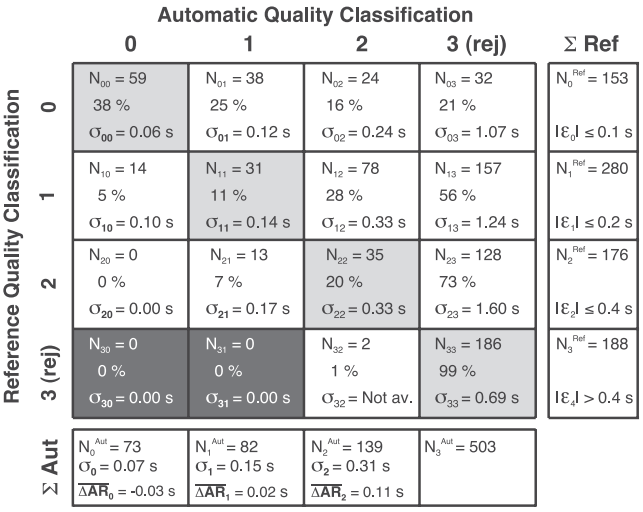

Figure 7. Performance of automatic *S*-wave picker (four quality classes) in matrix presentation similar to Di Stefano *et al.* (2006). The number of picks of reference class *i* classified by the automatic picker as class *j* is represented by N_{ij}. Percentages correspond to the number of automatic picks per reference quality class. Diagonal elements represent correctly classified automatic picks (reference and automatic weight are the same). Off-diagonal elements represent picks that were upgraded or downgraded by the automatic picker. N_i^{Ref} for each row is equal to the sum over *j* of the corresponding N_{ij}; N_j^{Aut} for each column is equal to the sum over *i* of the corresponding N_{ij}. The σ_{ij} denote the standard deviation of the difference ΔAR between automatic and reference pick for each matrix element. The ε_i refer to the error of quality class *i* used for reference picking. N_j^{Aut}, σ_j, and $\overline{\Delta\text{AR}}_j$ represent the number, standard deviation, and mean of ΔAR for all automatic picks classified as *j*, respectively. Note that none of the reference class 3 picks (rejected class) has been upgraded to high-quality class 0 or 1.

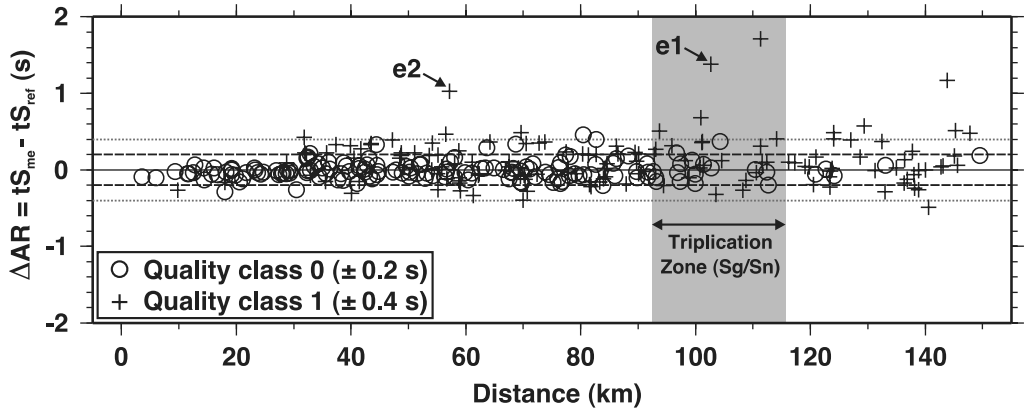

Figure 8. Difference between automatic and reference pick ΔAR against epicentral distance for usable automatic picks of class 0 (circles) and 1 (crosses) in simplified weighting scheme. Dashed lines represent the error interval of class 0 (±0.2 sec), and dotted lines indicate the error interval of class 1 (±0.4 sec). The number of gross outliers increase in the distance range of the triplication zone. In this distance range the first arriving weak *Sn* is followed by an impulsive *Sg*, and a mispick on a later phase is likely.

Diehl *et al.* (2009). Identified mispicks have to be removed from the data set.

Parameter Search Procedure. To derive a satisfactory picker performance for a certain data set, appropriate values of the parameters listed in Table 4 have to be evaluated from a trial-and-error procedure. The picker is applied to the reference data for each set of parameters, and its resulting performance has to be assessed as described in the previous section. To facilitate the parameter search, we provide some guidelines on how the parameters have to be evaluated.

The general parameters $\Delta_{\mathrm{epi}}^{\mathrm{max}}$ and Δ_{AIC_3} depend mainly on the Moho topography of a region and the data quality. Initial values can be estimated from the analysis of reference or routine picks versus epicentral distance. The break off of reliable *Sn* observations indicates $\Delta_{\mathrm{epi}}^{\mathrm{max}}$; the characteristic kink in regional travel-time curves indicates the approximate crossover distance Δ_{AIC_3}.

Subsequently, both detectors should be separately adjusted aiming at a compromise between hit rate and accuracy and at avoiding large numbers of false detections. As for the combined approach, the performance of detectors has to be checked against the reference data. The choice of Δst and Δlt mainly controls the degree of resolution of the CF. A lower resolution usually results in more stable detection. Time thresholds *tup* and *tdw* control the sensitivity of the detectors and depend mainly on the expected dominant frequency of the signal. For *tup* we suggest initial values between half and twice the smallest error interval ε_0 used for the reference picking. Because *tdw* accounts for short singularities in the CF, we suggest a value between 0 and *tup*. The water level *cw* should be estimated from a few high signal-to-noise *S* phases. Before choosing our preferred value of 0.06, we tested a range between 0 and 0.1 with our data set.

Because of the dynamic configuration of search windows in our AR-AIC picker, the choice of initial picking windows (Δ*gN* and Δ*gS*) and model windows (Δ*LN* and Δ*LS*) is less critical. The model and noise windows depend mainly on the maximum expected period, and the initial picking window can be estimated from the maximum deviation between predicted arrival and actual arrival time in the reference data. Values of about 0.5 –2 sec should be appropriate. The initial value of Δ_{AIC_1} can be estimate from the distance above which detectors become less reliable. Initially, it can also be set to Δ_{AIC_3} and then reduced stepwise until a satisfactory accuracy is achieved.

Initially, all parameters related to the quality assessment can be disabled by using a corresponding default value ($\Delta_{\mathrm{AIC}_2} = \Delta_{\mathrm{epi}}^{\mathrm{max}}$, minimum $S2N = 1$ for all classes, etc.). If the resulting performance does not fulfill the requirements, Δ_{AIC_2} should be gradually reduced. If there are still single mispicks present in the resulting automatic picks, certain minimum signal-to-noise thresholds have to be defined. Of course, highest quality classes should denote higher thresholds. After final consistency checks, like Wadati diagrams, additional V_P/V_S filters can be defined by κ_{min} and κ_{max}. Eventually, the performance for different frequency bands should be tested by applying specific waveform filters. Ⓔ Further information is provided in the supplement that is available in the electronic edition of *BSSA*.

Production Mode

In the production mode the calibrated automatic picker is applied to a data set of 552 local earthquakes in the Alpine region (white circles in Fig. 6). The majority of the approximately 13,300 *P* arrivals in this data set were picked with the MannekenPix (MPX) picking tool of Aldersons (2004) as described in Diehl *et al.* (2009). Predicted *S*-arrival times are calculated in the same one-dimensional velocity model used for the test mode. Within this data set, 4986 seismograms satisfy the minimum requirements for automatic *S*-phase picking (*P* pick available, 3C recording, and $\Delta_{\mathrm{epi}} \leq 150$ km).

Because our picking approach assumes the *S*-wave arrival before and close to the maximum horizontal amplitude y_{MHA}, it requires that spikes and clipped amplitudes are detected and removed from the data. We implemented a running average despiking routine and a clipping detector, which are applied prior to the picking procedure. Waveforms with clipped amplitudes are rejected by default. The despiking routine and the clipping detector were calibrated during the test mode. From the 4986 potential 3C recordings, 453 (9%) are rejected due to clipped amplitudes.

The production mode yields 1618 class 0 (± 0.2 sec) and 973 class 1 (± 0.4 sec) automatic picks. Hence, 57% of the (nonclipped) potential *S* phases could be picked with our approach. If outliers are disregarded, the average picking uncertainty amounts to about 0.27 sec. Because outliers are associated with errors up to several seconds, they lower the average accuracy of the automatic picks significantly. Ⓔ Therefore, outliers from the production mode have to be identified and removed from the data set as described in the supplement that is available in the electronic edition of *BSSA*. *S* picks indicating V_P/V_S ratios > 1.75 were cross checked against waveforms for distances > 50 km in a semiautomatic procedure to assess the number of outliers due to misinterpreted phases. From 450 analyzed automatic picks, 42 (9%) were identified as obvious mispicks or highly questionable automatic picks. Most of these mispicks resulted from phase misinterpretation analogous to example e1 in Figure 8 in the distance range of the triplication zone (90–110 km). The 42 clearly identified mispicks represent about 2% of all automatic picks.

Discussion and Conclusion

The approach presented in this work integrates three of the most commonly used techniques for automatic *S*-wave detection and picking. If applied independently, none of the described methods is able to provide robust automatic picks at local to regional distances. STA/LTA pickers are rather sensitive to later *P*-wave energy present in the coda, polarization pickers can fail due to uncertainty in rotation or an insufficient degree of linear polarization, and the reliability of AR-AIC pickers depends strongly on the setup of the corresponding search windows.

By combining different picking techniques we improve the stability of the automatic picking, and, in addition, we derive *in situ* information about timing uncertainty and phase identification of the automatic picks. Our automatic approach provides timing accuracy comparable with manually picked *S* arrivals. More important, classification of impulsive high-quality *S* waves agrees very well with the manual error assessment. Compared to the reference picks, emergent and complex *S* arrivals are classified rather conservatively by the automatic picker. On the other hand, only very few poor-quality *S* arrivals are upgraded by the automatic picker to usable quality classes. The conservative quality assessment of the automatic picker results in a lower number of usable picks but with less outliers as compared to the reference picks.

The number of automatic mispicks due to misinterpretation of impulsive later arrivals increases especially in the range of the crossover distance between the *Sg* and the *Sn* phase. Detectors, as well as predictive AR-AIC pickers, often miss the preceding weak *Sn* phase. The main difficulty for the predictive AR-AIC picker is the proper configuration of the noise and the signal model windows. If parts of the impulsive later arriving phase are included in the signal window, a detection of the preceding small *Sn* is usually impossible. A first step to overcome this problem is the proposed dynamic configuration of the windows utilizing additional information from the STA/LTA function. Although this method avoids already some of the misinterpretation, it still fails for a large number of *Sn* phases. A possible future approach could include an AR-modeling window, moving from the noise part toward the expected *Sn* signal as proposed, for example, by Bai and Kennett (2000). The onset of a seismic signal is then characterized by increased order and values of the AR coefficients. Furthermore, multivariate AR modeling might improve the success rate of the AR-AIC component. As an addition, the polarization analysis can be extended to include the uncertainty in the rotation angles and by the use of complex traces as suggested, for example, by Vidale (1986), Bai and Kennett (2001), or Greenhalgh *et al.* (2005). Such further developments might lead to an improved performance of the polarization detector at larger distances. Future extensions should also include adaptive techniques to facilitate the calibration of the presented approach. Accounting for the dominant frequencies of the signals and pattern recognition techniques might reduce the number of user-defined parameters.

The outliers present in the reference data demonstrate that incorrect identification of *S* phases (especially *Sn*) is also a significant problem in hand picked data sets. The implementation of CFs provided by detectors and AR modeling into routine picking tools could facilitate and improve the visual identification and picking of *S* waves.

The resolution and reliability of tomographic models is strongly dependent on the quality and consistency of the inverted arrival-time data. To derive consistent and large data sets for regional models we have to apply automated repicking to waveform data because routine phase data from different networks usually do not contain a common quality assessment. Considering the large amount of data necessary for high-resolution regional tomographic models, manually repicking of waveforms does not represent a feasible alternative. As mentioned before, the average accuracy of our automatic approach is comparable to the average accuracy of manually picked *S* arrivals. In three-dimensional body-wave tomography the minimum resolution of a velocity perturbation depends mainly on the model parametrization and the data error. A V_P/V_S perturbation of $+5\%$ within the midcrust in a volume of $25 \times 25 \times 15$ km results in an $S - P$ residual of $\Delta_{SP} = 0.29$ sec, assuming a background $V_P/V_S = 1.73$,

$V_P = 6.0$ km/sec, and a ray length of 20 km through the three-dimensional volume. This anomaly in V_P/V_S can only be resolved if the sum of the absolute observation errors in the *P*- and *S*-wave arrivals is smaller than Δ_{SP}. With the average picking uncertainty of 0.27 sec for automatic *S* picks in our application, it is certainly difficult to resolve anomalies in $V_P/V_S < 5\%$ if we assume a mean uncertainty of at least 0.1 sec in the *P*-arrival times.

Together with the MPX picking tool of Aldersons (2004), our approach offers the possibility to generate sets of high-quality *P*- and *S*-phase data suitable for local and regional tomography.

Data and Resources

The waveform data set of local earthquakes used in this study is described in further detail in Diehl *et al.* (2009). Reference picking was performed with the SeismicHandler package (Stammler, 1993) and most of the plots were generated using the Generic Mapping Tool of Wessel and Smith (1995). To obtain an implementation of the presented *S*-picking algorithm, send a request to the authors.

Acknowledgments

We are grateful to the following networks in the Alpine Region who provided us with digital recordings used in this study: BED (Ludwig-Maximilians University, Munich), GERESS (Hannover), GRSN/SZGRF (Erlangen), INGV/MEDNET (Rome), LEDBW (Freiburg i. B.), OGS/CRS (Udine/Trieste), RENASS (Strasbourg), RSNI/DipTeris (Genova), SED (Zurich), SISMALP (Grenoble), SNRS (Ljubljana), TGRS (Nice), and ZAMG (Vienna). We thank S. Greenhalgh, J. Pujol, A. Cichowicz, and one anonymous reviewer whose thoughtful remarks and recommendations greatly improved the manuscript.

References

Akaike, H. (1973). Information theory and an extension of the maximum likelihood principle, in *Proc. of the 2nd International Symposium on Information Theory*, B. N. Petrov and F. Csaki (Editors), Akademiai Kiado, Budapest, 267–281.

Akazawa, T. (2004). A technique for automatic detection of onset time of *P* and *S* phases in strong motion records, in *Proc. of the 13th World Conf. on Earthquake Engineering*, Vancouver, Canada, Paper No. 786.

Aldersons, F. (2004). Toward three-dimensional crustal structure of the Dead Sea region from local earthquake tomography, *Ph.D. Thesis*, Tel Aviv University, Israel.

Allen, R. V. (1978). Automatic earthquake recognition and timing from single traces, *Bull. Seismol. Soc. Am.* **68,** 1521–1531.

Allen, R. V. (1982). Automatic phase pickers: their present use and future prospects, *Bull. Seismol. Soc. Am.* **72,** S225–S242.

Baer, M., and U. Kradolfer (1987). An automatic phase picker for local and teleseismic events, *Bull. Seismol. Soc. Am.* **77,** 1437–1445.

Bai, C. Y., and B. L. N. Kennett (2000). Automatic phase-detection and identification by full use of a single three-component broadband seismogram, *Bull. Seismol. Soc. Am.* **90,** 187–198.

Bai, C. Y., and B. L. N. Kennett (2001). Phase identification and attribute analysis of broadband seismograms at far-regional distances, *J. Seism.* **5,** 217–231.

Berger, J., and R. L. Sax (1980). Seismic detectors: the state of the art, Technical Report SSR-R-80-4588.

Christensen, N. I. (1996). Poisson's ratio and crustal seismology, *J. Geophys. Res.* **101,** 3139–3156.

Cichowicz, A. (1993). An automatic *S*-phase picker, *Bull. Seismol. Soc. Am.* **83,** 180–189.

Di Stefano, R., F. Aldersons, E. Kissling, P. Baccheschi, C. Chiarabba, and D. Giardini (2006). Automatic seismic phase picking and consistent observation error assessment: application to the Italian seismicity, *Geophys. J. Int.* **165,** 121–134, doi 10.1111/j.1365-246X.2005.02799.x.

Diehl, T., E. Kissling, S. Husen, and F. Aldersons (2009). Consistent phase picking for regional tomography models: application to the greater Alpine region, *Geophys. J. Int.* **176,** 542–554, doi 10.1111/j.1365-246X.2008.03985.x.

Flinn, E. A. (1965). Signal analysis using rectilinearity and direction of particle motion, *Proc. IEEE* **53,** 1874–1876.

Goes, S., R. Govers, and P. Vacher (2000). Shallow mantle temperatures under Europe from *P*- and *S*-wave tomography, *J. Geophys. Res.* **105,** 11,153–11,169.

Gomberg, J. S., K. M. Shedlock, and S. W. Roecker (1990). The effect of *S*-wave arrival times on the accuracy of the hypocenter estimation, *Bull. Seismol. Soc. Am.* **80,** 1605–1628.

Greenhalgh, S., M. Mason, and B. Zhou (2005). An analytical treatment of single station triaxial seismic direction finding, *J. Geophys. Eng.* **2,** 8–15.

Holbrook, W. S., W. D. Mooney, and N. I. Christensen (1992). The seismic velocity structure of the deep continental crust, in *The Continental Lower Crust*, D. M. Fountain, R. Arculus and R. W. Kay (Editors), Elsevier, Amsterdam, 1–43.

Husen, S., E. Kissling, E. R. Flueh, and G. Asch (1999). Accurate hypocentre determination in the seismogenic zone of the subducting Nazca plate in northern Chile using a combined on/offshore network, *Geophys. J. Int.* **105,** 687–701.

Kissling, E. (1988). Geotomography with local earthquake data, *Rev. Geophys.* **26,** 659–698.

Kisslinger, C., and E. R. Engdahl (1973). The interpretation of the Wadati diagram with relaxed assumptions, *Bull. Seismol. Soc. Am.* **63,** 1723–1736.

Kitagawa, G., and H. Akaike (1978). A procedure for the modeling of non-stationary time series, *Ann. Inst. Stat. Math.* **30,** 351–363.

Leonard, M., and B. L. N. Kennett (1999). Multi-component autoregressive techniques for the analysis of seismograms, *Phys. Earth Planet. Inter.* **113,** 247–263.

Maurer, H., and U. Kradolfer (1996). Hypocentral parameters and velocity estimation in the western Swiss Alps by simultaneous inversion of *P*- and *S*-wave data, *Bull. Seismol. Soc. Am.* **86,** 32–42.

Montalbetti, J. R., and E. R. Kanasewich (1970). Enhancement of teleseismic body phases with a polarization filter, *Geophys. J. R. Astr. Soc.* **21,** 119–129.

Plešinger, A., M. Hellweg, and D. Seidl (1986). Interactive high-resolution polarization analysis of broadband seismograms, *J. Geophys.* **59,** 129–139.

Ruud, B. O., and E. S. Husebye (1992). A new three-component detector and automatic single station bulletin production, *Bull. Seismol. Soc. Am.* **82,** 221–237.

Samson, J. C. (1977). Matrix and stokes vector representations of detectors for polarized waveforms: theory, with some applications to teleseismic waves, *Geophys. J. R. Astr. Soc.* **51,** 583–603.

Sleeman, R., and T. van Eck (1999). Robust automatic *P*-phase picking: an online implementation in the analysis of broadband seismogram recordings, *Phys. Earth Planet. Inter.* **113,** 265–275.

Stammler, K. (1993). SeismicHandler—programmable multichannel data handler for interactive and automatic processing of seismological analysis, *Comp. Geosci.* **19,** 135–140.

Takanami, T., and G. Kitagawa (1988). A new efficient procedure for the estimation of onset times of seismic waves, *J. Phys. Earth* **36,** 267–290.

Takanami, T., and G. Kitagawa (1991). Estimation of the arrival times of seismic waves by multivariate time series models, *Ann. Inst. Stat. Math.* **43,** no. 3, 407–433.

Takanami, T., and G. Kitagawa (1993). Multivariate time-series models to estimate the arrival times of *S* waves, *Comp. Geosci.* **19,** 295–301.

Vidale, J. E. (1986). Complex polariszation analysis of particle motion, *Bull. Seismol. Soc. Am.* **76,** 1393–1405.

Wang, J., and T. Teng (1997). Identification and picking of *S* phase using an artificial neural network, *Bull. Seismol. Soc. Am.* **87,** no. 5, 1140–1149.

Wessel, P., and W. H. F. Smith (1995). New version of the Generic Mapping Tool released, *EOS Trans. AGU* **76,** 329.

Zhang, H., C. H. Thurber, and C. A. Rowe (2003). Automatic *P*-wave arrival detection and picking with multiscale wavelet analysis for single-component recordings, *Bull. Seismol. Soc. Am.* **93,** 1904–1912.

Institute of Geophysics
ETH Zurich, Switzerland
tdiehl@ldeo.columbia.edu
(T.D., E.K.)

Swiss Seismological Service
ETH Zurich, Switzerland
(N.D., S.H.)

Manuscript received 3 April 2008